

## Supplementary Information

### Efficient MA-Free Perovskite Solar Cells with Balanced Carrier Transport Achieved by 4-Trifluorophenylammonium Iodide

Linrui Li,<sup>a, b</sup> Yinhua Lv, <sup>\*,b, c</sup> Qianlong Liu,<sup>b</sup> Zhenghui Fan,<sup>b</sup> Ruihan Yuan,<sup>b</sup> Weijian Tang,<sup>a</sup> Xinhang Liu,<sup>b</sup> Ping Zhang,<sup>\*,a</sup> and Wen-Hua Zhang <sup>\*,b, c</sup>

<sup>a</sup> College of Materials Science and Engineering, Sichuan University, 24 First South Section First Ring Road, Chengdu, 610064, China

<sup>b</sup> Sichuan Research Center of New Materials, Institute of Chemical Materials, China Academy of Engineering Physics, 596 Yinhe Road, Shuangliu, Chengdu, 610200, China

<sup>c</sup> School of Materials and Energy, Yunnan University, Kunming 650500, China

\* Corresponding author.

E-mail: [qiehahah@163.com](mailto:qiehahah@163.com) (Y. Lv); [zhp@scu.edu.cn](mailto:zhp@scu.edu.cn) (P. Zhang); [whzhang@caep.cn](mailto:whzhang@caep.cn) ; [wenhuazhang@ynu.edu.cn](mailto:wenhuazhang@ynu.edu.cn) (W-H. Zhang)

# Experimental section

## Materials.

Fluorine-doped tin oxide (FTO) glass substrates which resistance was  $14 \Omega \text{ sq}^{-1}$  were purchased from Beijing Huamin New Materials Technology Co. Ltd. Cesium iodide (CsI; 99.999%) was obtained from Alfa Aesar. Formamidinium iodide (FAI; 99.5%), formamidinium bromide (FABr; 99.5%), lead iodide ( $\text{PbI}_2$ ; 99.99%), lead chlorine ( $\text{PbCl}_2$ ; 99.99%), 2,2',7,7'-tetrakis-(*N*, *N*-di-*p*-methoxyphenyl-amine)-9,9'-spirobifluorene (spiro-OMeTAD; 99.8%), poly[bis(4-phenyl) (2,4,6-trimethylphenyl)-amine] (PTAA, Mw = 17000) and 4-trifluorophenyl ammonium iodide (TFPAI; 99.5%) were purchased from Xi'an Polymer Light Technology. Dimethyl formamide (DMF; 99.8%), dimethyl sulfoxide (DMSO; 99.8%), isopropanol (IPA; 99.5%), and chlorobenzene (CB; 99.5%) were acquired from Aladdin. 4-isopropyl-4'-methyldiphenyliodonium tetrakis (pentafluorophenyl) borate (TPFB) was obtained from TCI Co. Ltd. All materials were used without any further purification.

## Device fabrication.

The patterned FTO glass substrates were cleaned ultrasonically in acetone, isopropyl alcohol, ethanol, deionized water each for 30 min, sequentially. The compact  $\text{TiO}_2$  layer was fabricated by using hydrothermal treatment of 0.2 M  $\text{TiCl}_4$  at 70 °C for 70 min. The treated films were washed with deionized water, ethanol and then dried in 70 °C oven for 2h. Before using, the FTO/ $\text{TiO}_2$  substrates were annealed at 150 °C for 30 min and treated with UV ozone for 15 min to improve the wettability. Afterwards, the perovskite layer was prepared through anti-solvent processed spin coating method in a  $\text{N}_2$ -filled glovebox. For the 1.4 M  $\text{Cs}_{0.15}\text{FA}_{0.85}\text{Pb}(\text{I}_{0.95}\text{Br}_{0.03}\text{Cl}_{0.02})_3$  perovskite (~1.56 eV) precursor solutions, 52.6 mg of CsI, 185.7 mg of FAI, 8.4 mg of FABr, 591.3 mg of  $\text{PbI}_2$ , 18.8 mg of  $\text{PbCl}_2$  were dissolved in 1 mL DMF/DMSO (4/1 v/v) mixed solvent. The precursor solution was spin-coated onto the FTO/ $\text{TiO}_2$  substrate at 1000 rpm for 10s and 4000 rpm for 30 s, and 110  $\mu\text{L}$  of anisole was dripped onto the substrate at 10s

before the end. Then the perovskite layers were annealed at 110 °C for 20 min. When the perovskite films were cooled to room temperature, different ratio (5, 7, 9, 11,13 mg·mL<sup>-1</sup>) TFPAI solution dissolved in isopropyl alcohol were spin-coated onto the compact TiO<sub>2</sub> substrates at 5000 rpm for 30s, respectively. The spiro-OMeTAD solution was prepared by 72.3 mg·mL<sup>-1</sup> spiro-OMeTAD in chlorobenzene with 28.8 μL of 4-tert-butylpyridine and 17.5 μL of Li-TFSI solution (520 mg·mL<sup>-1</sup> in acetonitrile), and spin-coated at 4000 rpm 30 s. Finally, 80 nm Au back electrode was deposited by thermal evaporation. The initial active area was 0.09 cm<sup>2</sup>. For the (TFPA)<sub>2</sub>FA<sub>n-1</sub>Pb<sub>n</sub>I<sub>3n+1</sub> perovskite, TFPAI, FAI, and PbI<sub>2</sub> (molar ratio of 2: (n-1): n) were dissolved in 1 mL DMF/DMSO (4/1 v/v) mixed solvent for 0.4 M precursor solution. Then the solution was spin-coated onto the FTO/TiO<sub>2</sub> substrate at 2000 rpm for 30 s without the drip of antisolvent, then the layers were annealed at 40 °C for 1 min. For thermal stability test, the PTAA solution (20 mg·mL<sup>-1</sup> in chlorobenzene) with additives of 20 μL of TPFB solution (100 mg·mL<sup>-1</sup> in acetonitrile) was spin-coated onto perovskite layer at 5000 rpm 30 s as a substitute for the spiro-OMeTAD layer.

### Characterizations.

The top-viewed and the cross-sectional SEM images were obtained by using a Hitachi SU8020 field-emission scanning electron microscopy (Hitachi High Technologies Corporation). A Fourier transform infrared spectroscopy (FTIR, TENSOR 27) was used to collect the FTIR spectral data for the samples without and with TFPAI treatment. The sample was coated on KBr pellet. X-ray diffraction (XRD) patterns were recorded by a D8 X-ray diffractometer (X' pert Pro-1), employing Cu K<sub>α</sub> as incident radiation. Photovoltaic performance of solar cells was measured under illumination of simulated sunlight (standard AM 1.5G, 100 mW·cm<sup>-2</sup>, SSF5-3A, Enlitech), and the *J-V* curves were recorded using a Keithley digital source meter (Model 2400), the light intensity of the solar simulator was calibrated by a standard silicon solar cell provided by PV Measurements. The active area of the solar cells was confirmed by using a metal aperture of 0.09 cm<sup>2</sup> to avoid light scattering through the sides. The *J-V* curves for the devices were measured by forward (-0.1 V to 1.2 V

forward bias) or reverse (1.2 V to -0.1 V) scans with a scan rate of 100 mV/s. The external quantum efficiencies (EQE) were measured in AC mode by a QE-R3011 testing system (Enlitech). For XPS measurement, radiation was produced by a monochromatic 75 W Al K<sub>α</sub> excitation centered at 1486.7 eV. The PL measurements were performed with time-correlated single photon counting (TCSPC) with a 508 nm laser (DD-510L, Deltaflex, Horiba). The space-charge limited current (SCLC), electrochemical impedance Spectroscopy (EIS) and Mott-Schottky (M-S) analysis were conducted by using a multi-channel potentiometer (VMP3, Biologic) under dark conditions. EIS data were recorded at 0 and 0.6 V in the frequency range from 1 MHz to 50 mHz with an AC amplitude of 50 mV. The Mott-Schottky data were recorded at the frequency of 1 KHz in the applied voltage range from -0.1 V to 1.2 V with an AC amplitude of 20 mV.

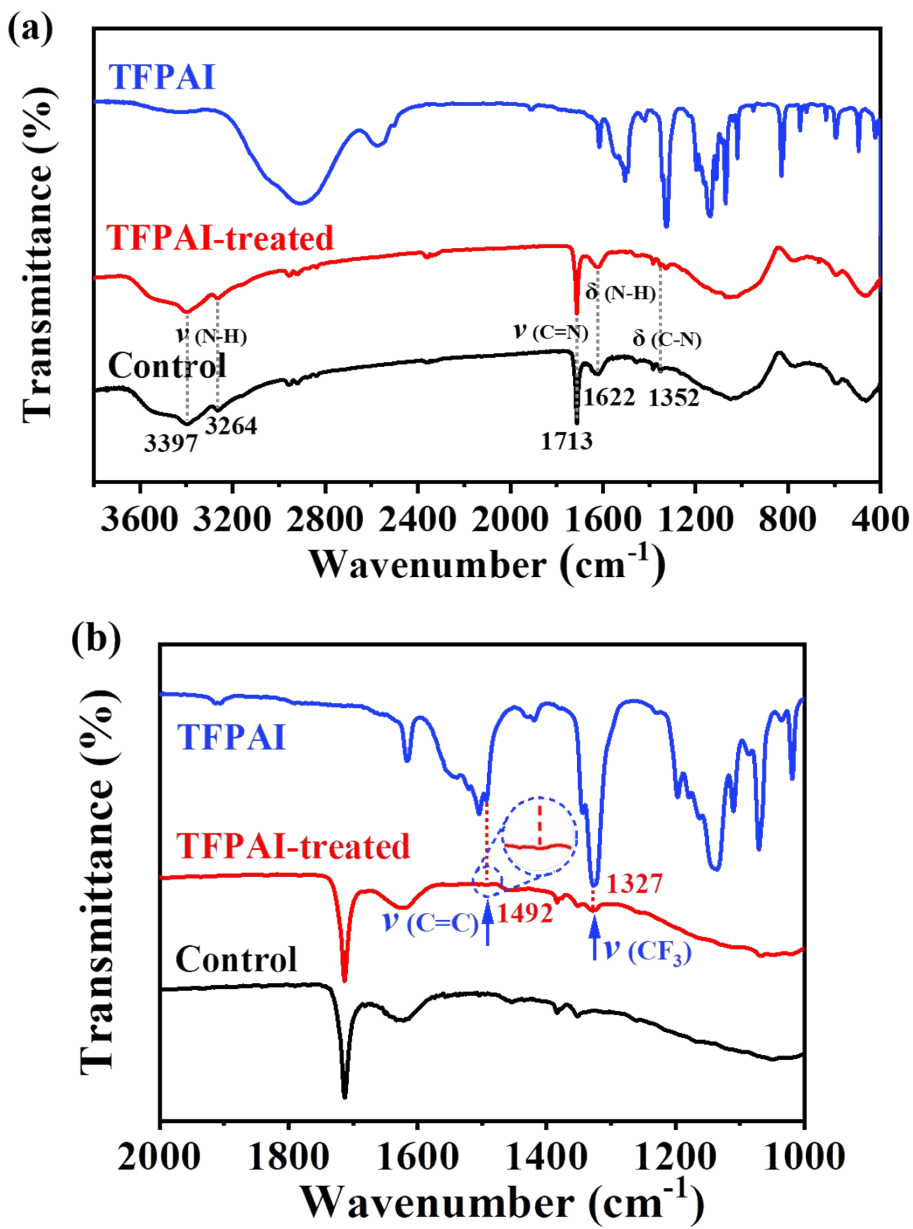


**Fig. S1** (a) The FTIR spectra of TFPAl, the perovskite without and with TFPAl treatment and (b) its partially enlarged FTIR patterns in the wavenumber range from 2000 to 1000  $\text{cm}^{-1}$ .

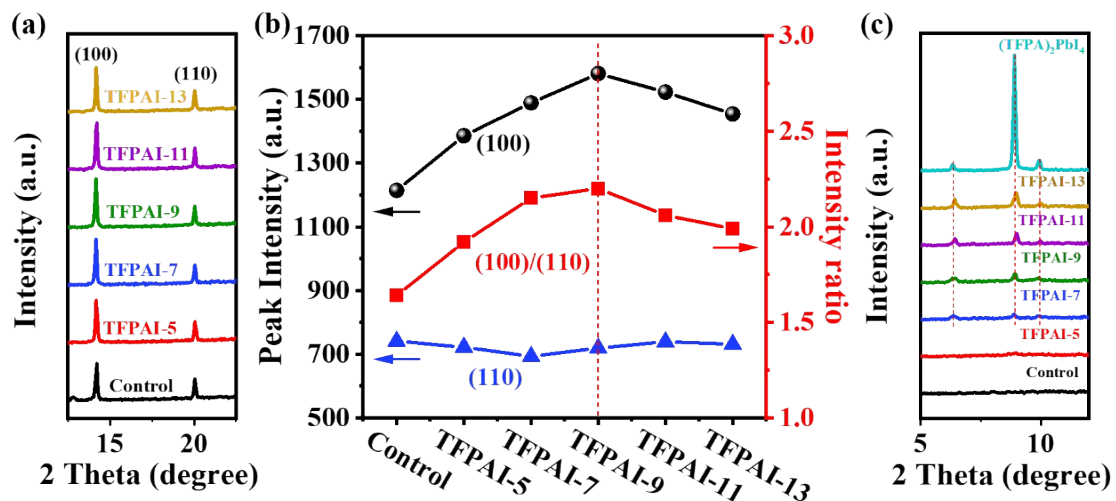


**Fig. S2** (a) Partially enlarged XRD patterns in the range of 12.5-22.5°. (b) The diffraction intensity ratio between (100) plane and (110) plane. (c) Partially enlarged XRD patterns at low diffraction angle area.

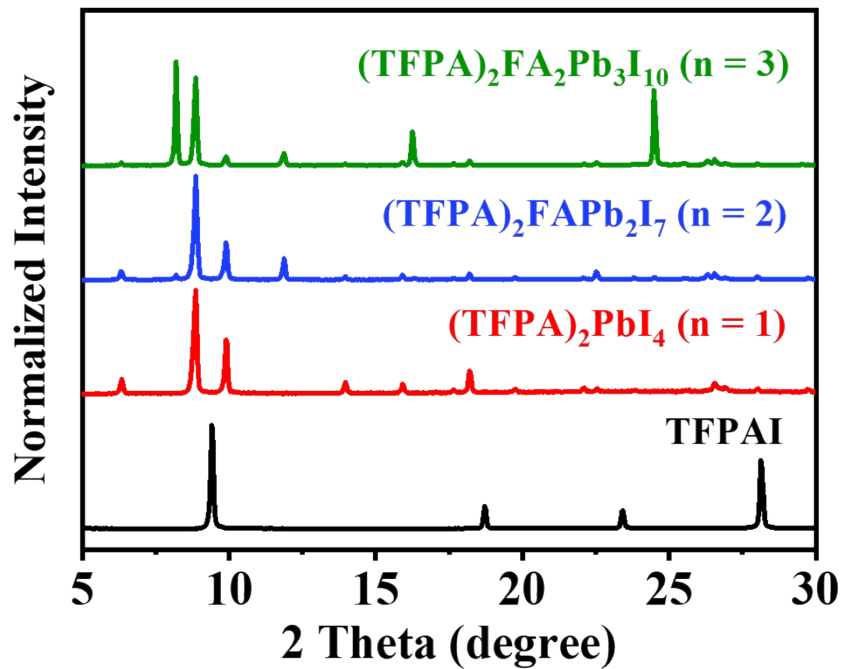
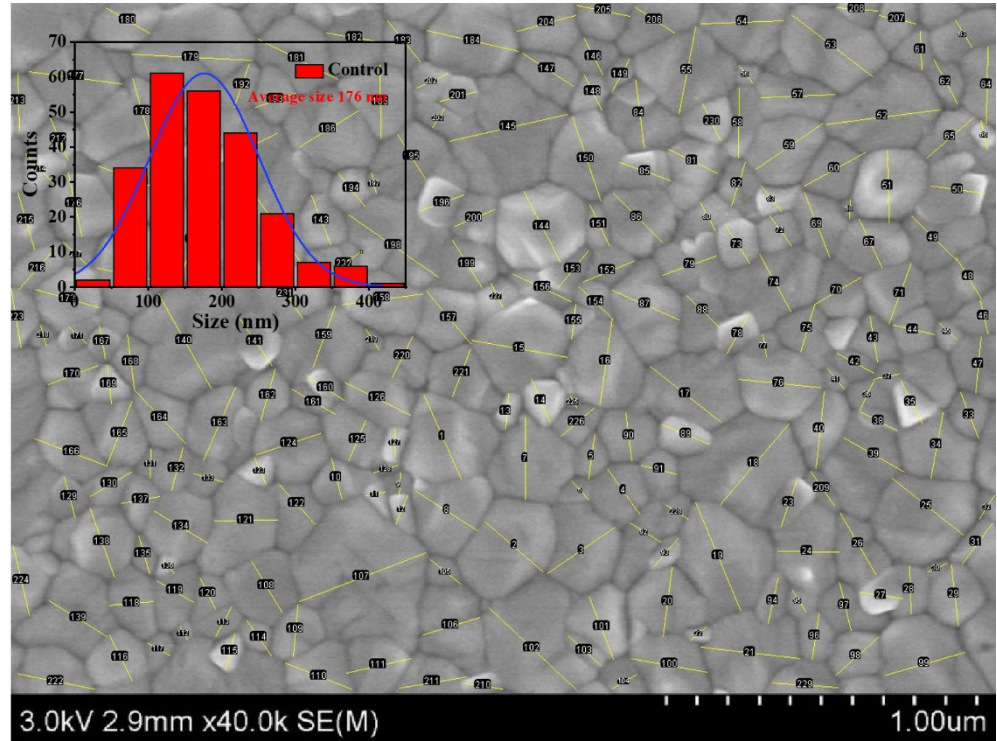


**Fig. S3** The XRD patterns of different  $n$  values  $(TFPA)_2FA_{n-1}Pb_nI_{3n+1}$  perovskite films fabricated by following the corresponding stoichiometric ratio.

**(a)**



**(b)**

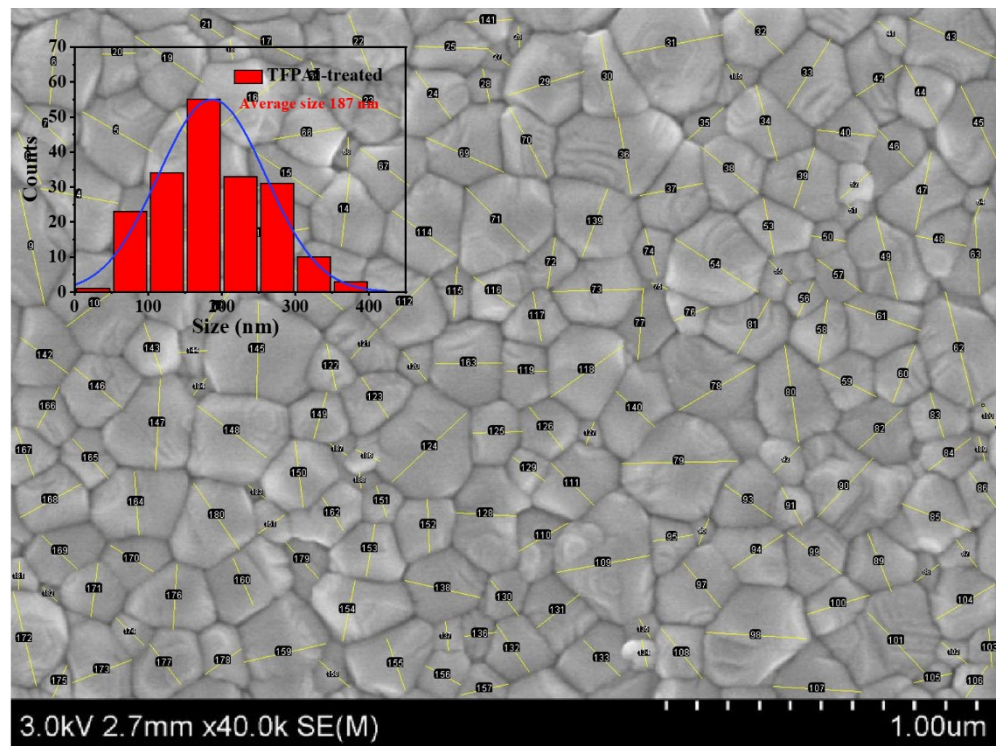


**Fig. S4** The grain sizes distribution statistics of perovskite films (a) without and (b) with TFPAI treatment.

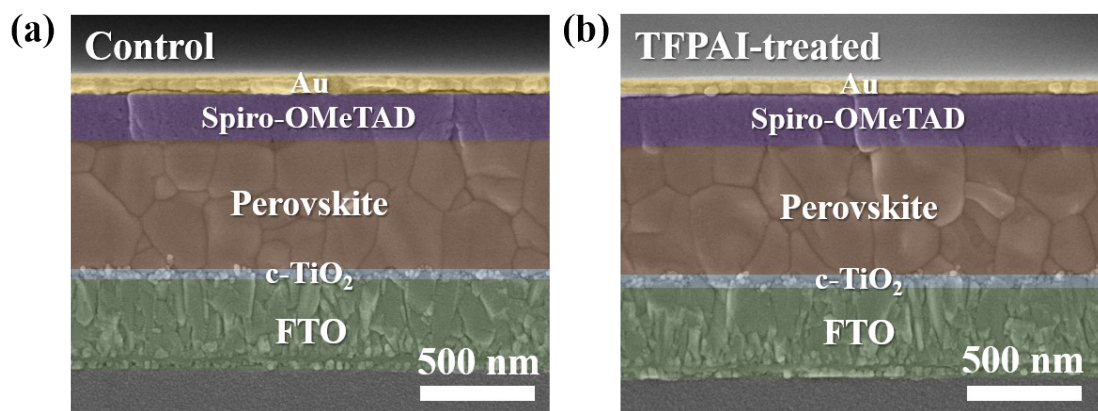


**Fig. S5** Cross-sectional SEM images of PSC devices (a) without and (b) with TFPAL treatment.

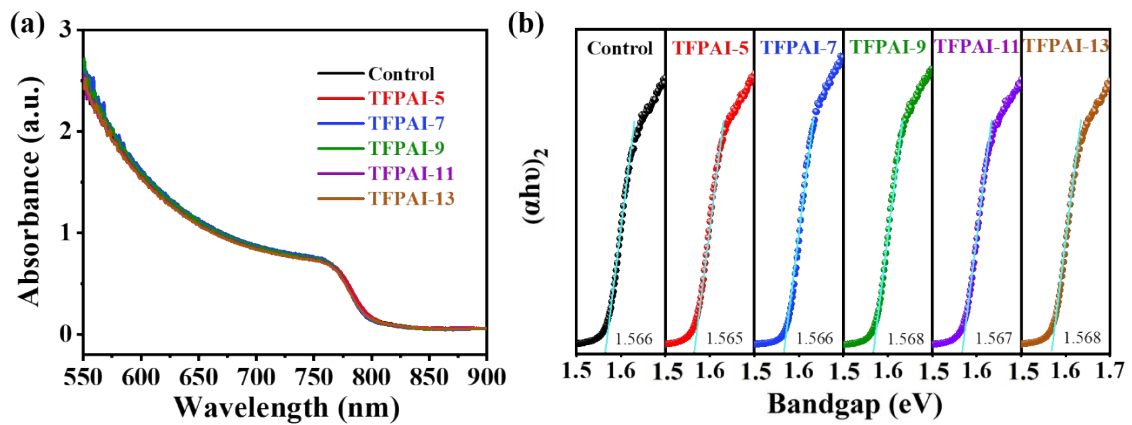


**Fig. S6** (a) The UV-Vis absorption spectra of perovskite films with different TFPAl-treated concentrations and (b) the corresponding bandgaps ( $\sim 1.57$  eV).

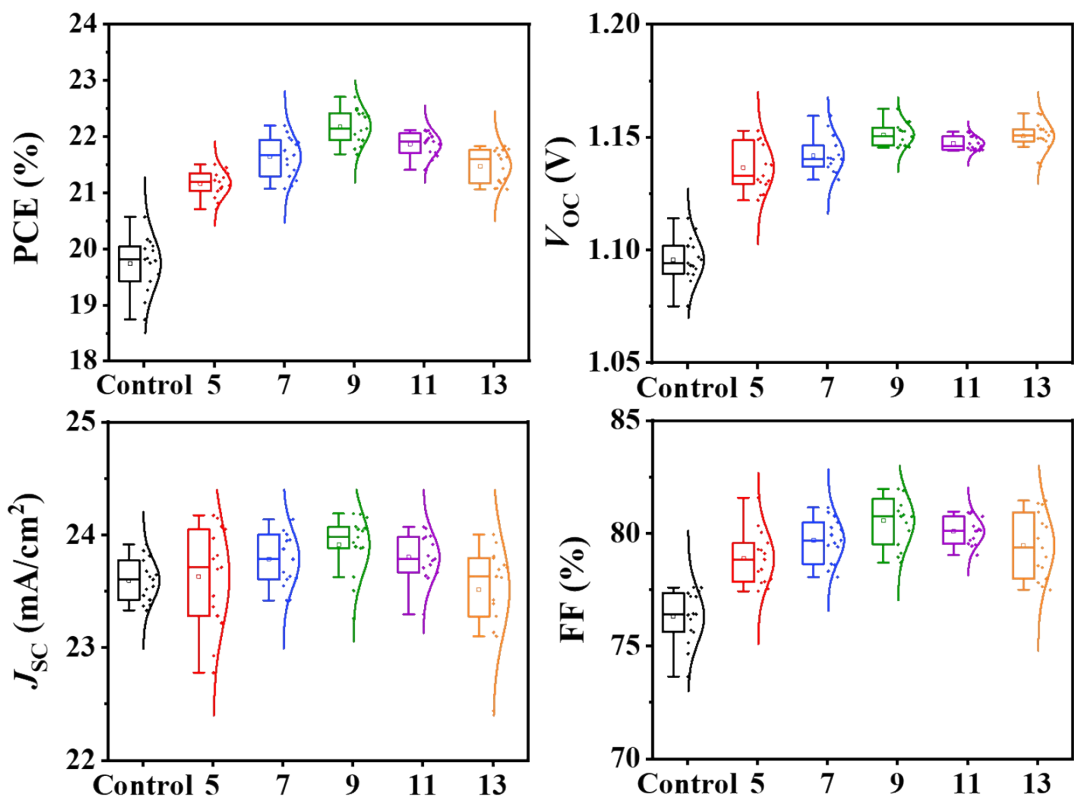


**Fig. S7** Statistics of PV parameters (PCE,  $V_{OC}$ ,  $J_{SC}$ , and FF) for the devices based on the perovskite films with different TFPAl-treated concentrations.

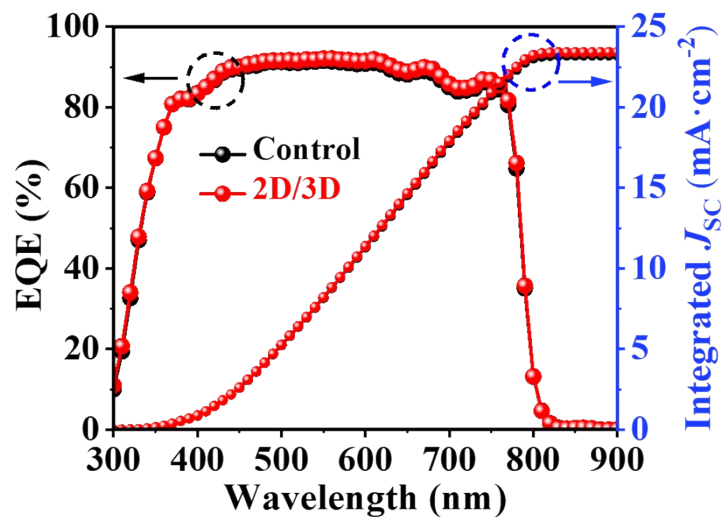


**Fig. S8** EQE spectra and integrated  $J_{SC}$  for the control and 2D/3D devices.

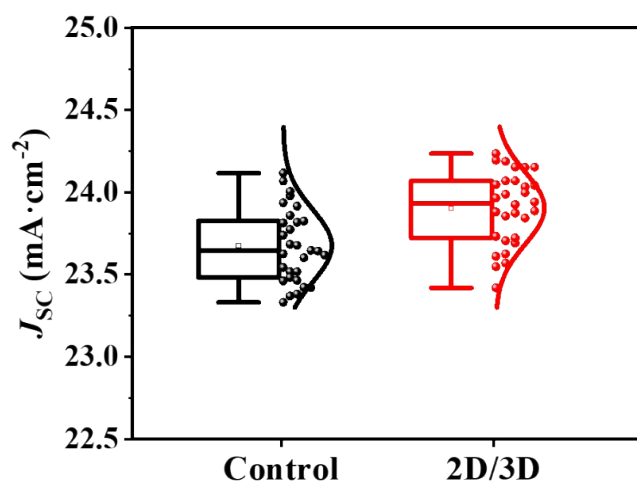


**Fig. S9** Statistics of  $J_{SC}$  for the control and 2D/3D devices.

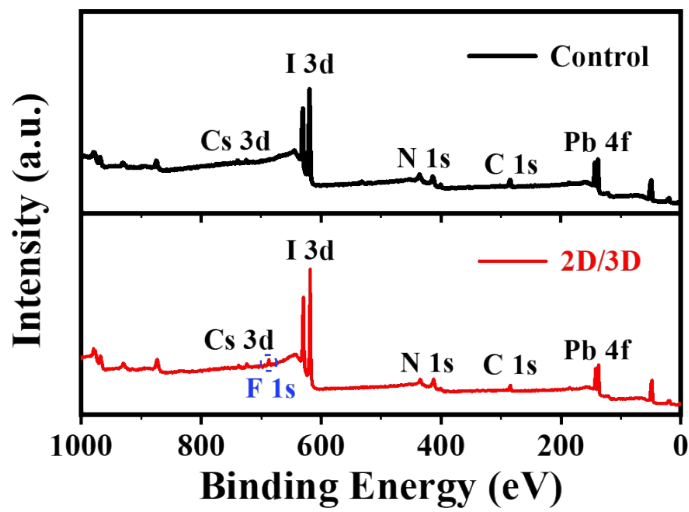


**Fig. S10** The survey XPS spectra of the control and 2D/3D perovskite films.

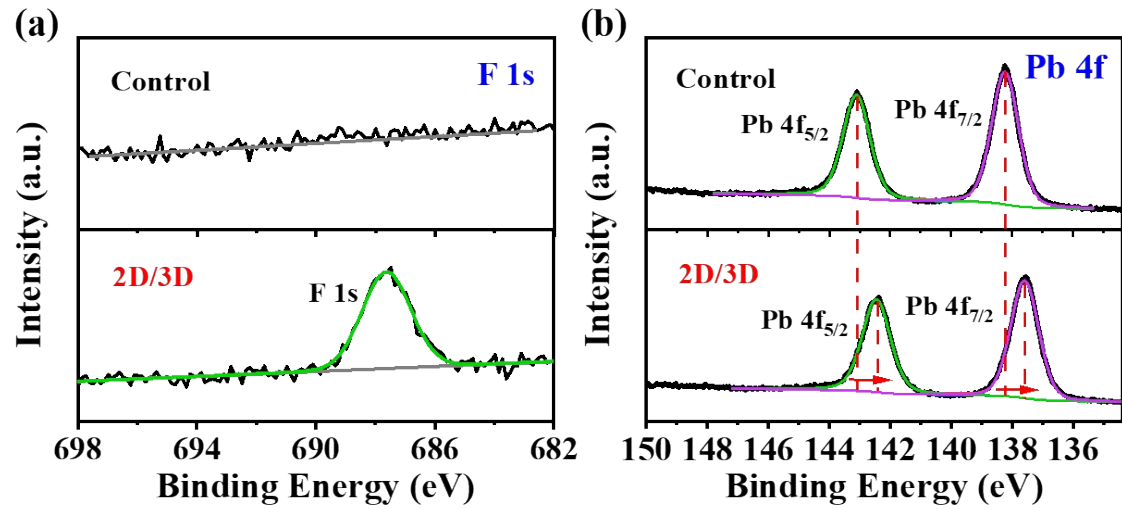


**Fig. S11** XPS spectra of (a) F 1s and (b) Pb 4f for the control and 2D/3D films, respectively.

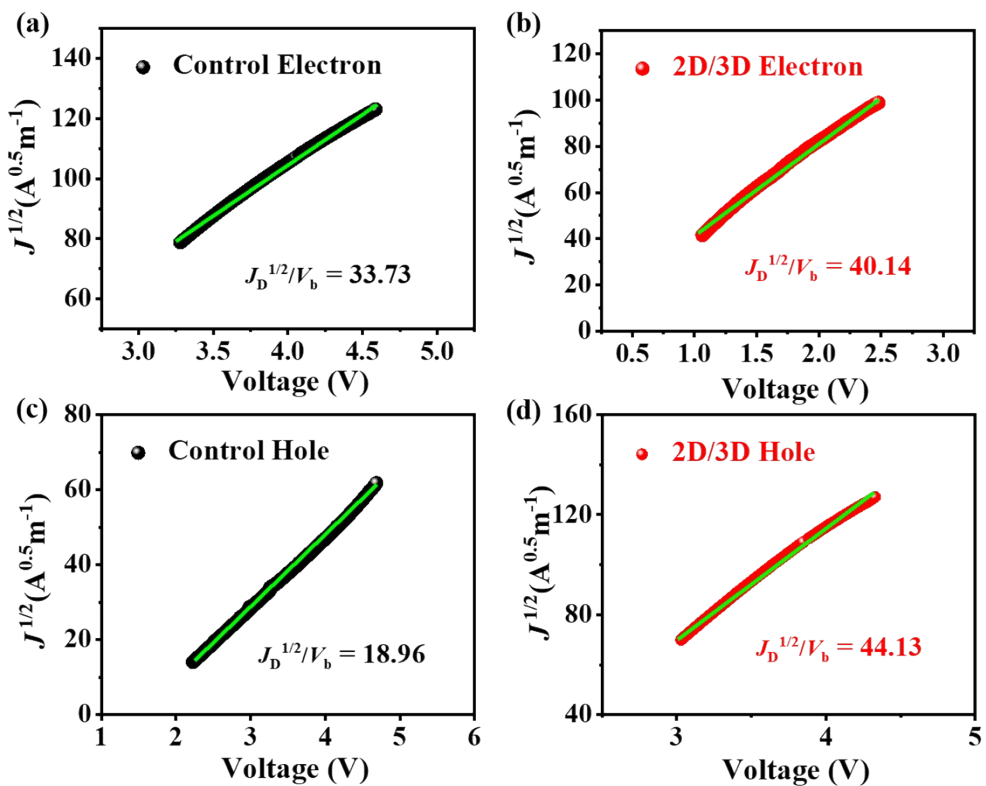


**Fig. S12**  $J^{1/2}$ - $V$  plots for the (a-b) electron-only and (c-d) hole-only devices based on the control and 2D/3D perovskites.

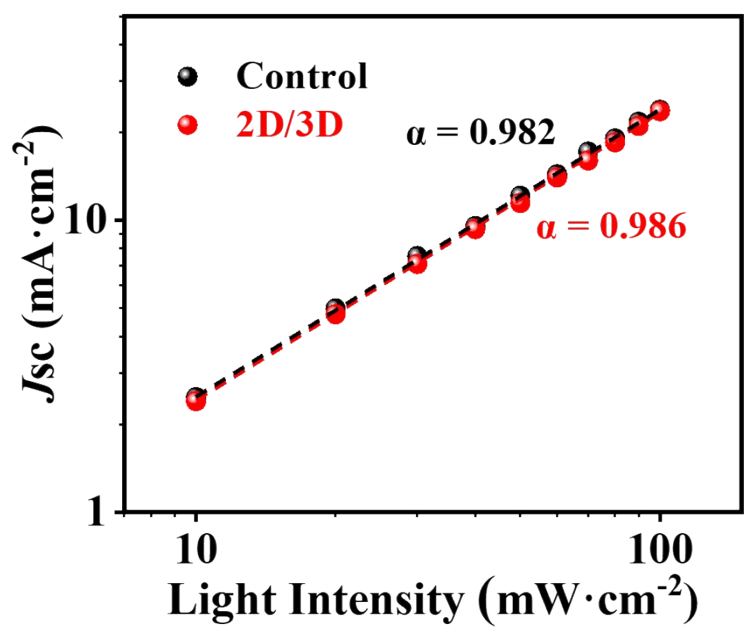
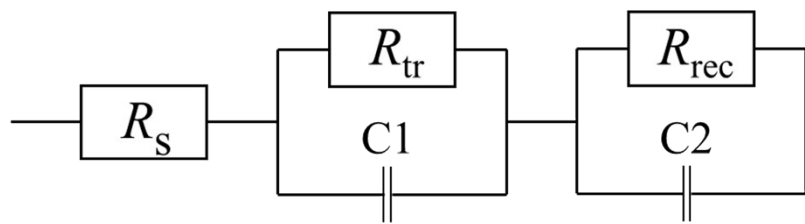
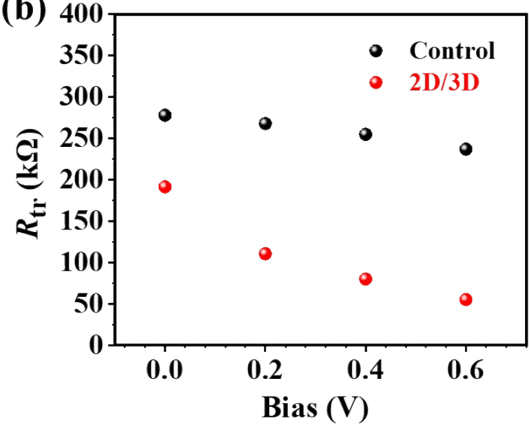


**Fig. S13**  $J_{SC}$  vs. light intensity for the control and 2D/3D devices.

(a)



(b)



(c)

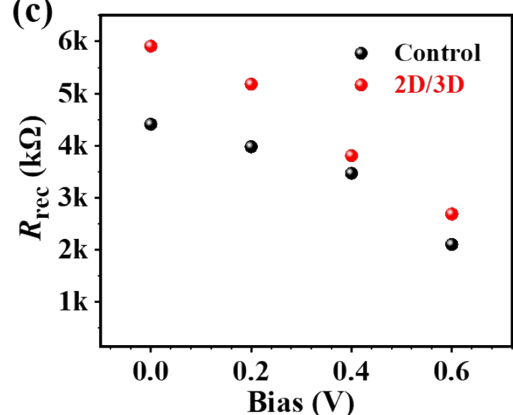


**Fig. S14** (a) The equivalent circuit of the Nyquist plots. (b)  $R_{\text{tr}}$  and (c)  $R_{\text{rec}}$  fitted from the Nyquist plots.

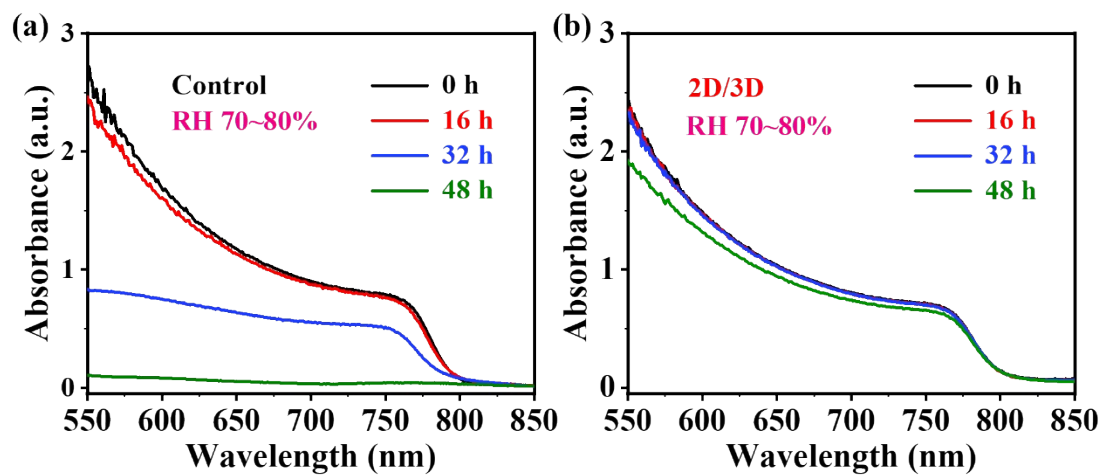


**Fig. S15** UV-vis spectra of the (a) control and (b) 2D/3D films at different time under RH = 70 ~ 80% environment

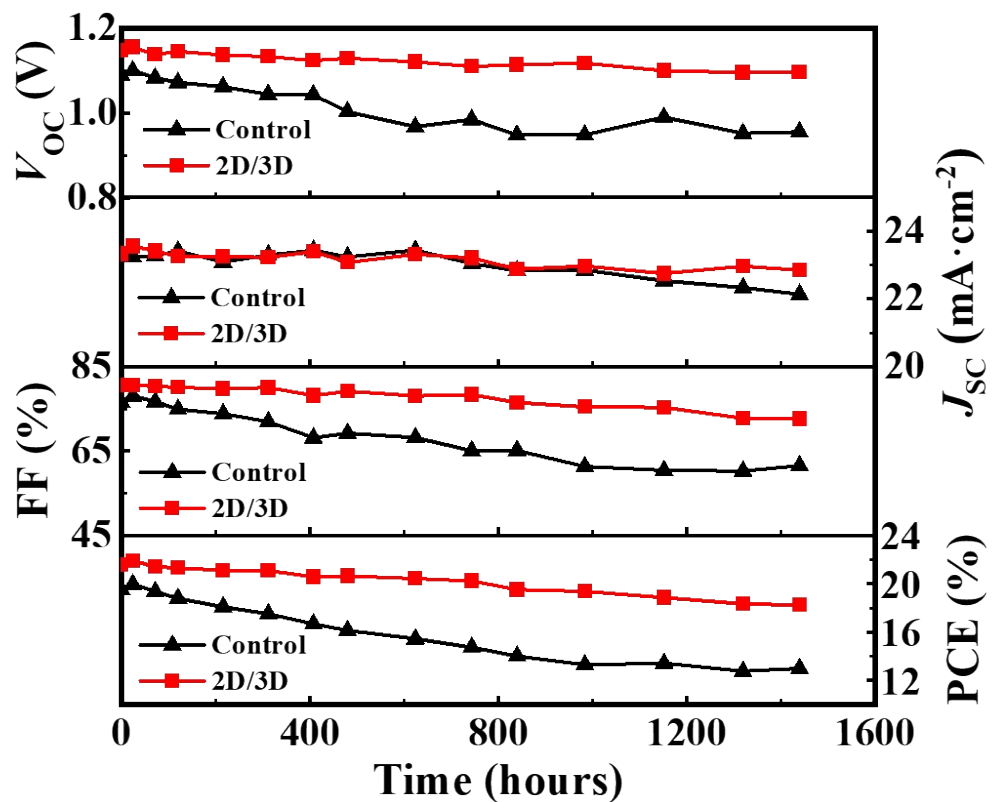


**Fig. S16** The corresponding variation of  $V_{OC}$ ,  $J_{SC}$ , FF, and PCE parameters for the control and 2D/3D devices under  $\text{RH} = 35 \pm 5\%$  ambient air condition.

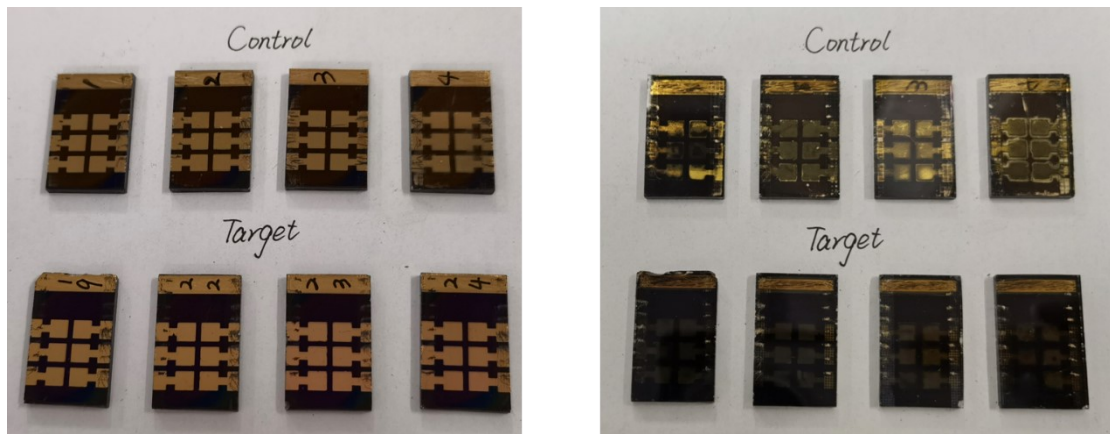


**Fig. S17** (a) Front and (b) back pictures of the control and 2D/3D films after humidity stability test ( $\text{RH} = 35 \pm 5\%$ , 60 days).

**Table S1** Summary of photovoltaic parameters of 2D/3D perovskite solar cells.

Method: Adding organic ammonium salt into precursor							
Year	Device structures	Organic ammonium salt	V <sub>OC</sub> (V)	J <sub>SC</sub> (mA·cm <sup>-2</sup> )	FF	PCE (%)	Ref.
2017	FTO/c-TiO <sub>2</sub> /m-TiO <sub>2</sub> / <b>MAPbI<sub>3</sub></b> /spiro-OMeTAD/Au	AVAI	1.03	18.8	0.76	14.6	1
2017	FTO/(SnO <sub>2</sub> /PCBM)/ <b>Cs<sub>x</sub>FA<sub>1-x</sub>PbBr<sub>y</sub>I<sub>3-y</sub></b> /spiro-OMeTAD/Au	BAI	1.14	22.7	0.80	20.6	2
2018	FTO/c-TiO <sub>2</sub> /m-TiO <sub>2</sub> / <b>MAPbI<sub>3</sub></b> /spiro-OMeTAD/Au	PEAI	1.08	21.9	0.80	19.1	3
2018	FTO/c-TiO <sub>2</sub> /m-TiO <sub>2</sub> /						
2018	<b>(FAPbI<sub>3</sub>)<sub>0.85</sub>(MAPbBr<sub>3</sub>)<sub>0.15</sub></b> /spiro-OMeTAD/Au	EAI	1.10	22.2	0.77	18.8	4
2018	FTO/SnO <sub>2</sub> / <b>Cs<sub>0.05</sub>(FA<sub>0.83</sub>MA<sub>0.17</sub>)<sub>0.95</sub>Pb(I<sub>0.83</sub>Br<sub>0.17</sub>)<sub>3</sub></b> /spiro-OMeTAD/Au	EDBEI <sub>2</sub>	1.11	23.2	0.75	19.1	5
2018	FTO/TiO <sub>2</sub> / <b>Cs<sub>x</sub>FA<sub>1-x-y</sub>MA<sub>y</sub>PbI<sub>3-z</sub>Br<sub>z</sub></b> /spiro-OMeTAD/Au	A <sub>43</sub>	1.11	22.9	0.79	20.1	6
2018	ITO/SnO <sub>2</sub> / <b>CsPbI<sub>x</sub>Br<sub>3-x</sub></b> /spiro-OMeTAD/Au	PEAI	1.07	16.6	0.70	12.4	7
2019	ITO/SnO <sub>2</sub> / <b>FA<sub>x</sub>MA<sub>1-x</sub>PbI<sub>3-y</sub>Cl<sub>y</sub></b> /spiro-OMeTAD/(MoO <sub>3</sub> /Ag)	ThMAI	1.16	22.9	0.81	21.5	8
2020	ITO/SnO <sub>2</sub> /ZnO <sub>2</sub> / <b>Cs<sub>x</sub>FA<sub>1-x</sub>PbI<sub>3</sub></b> /spiro-OMeTAD/Ag	β-GUA	1.14	24.4	0.80	22.2	9
2020	ITO/SnO <sub>2</sub> / <b>5F-</b>						
2020	<b>PA<sub>0.05</sub>[Cs<sub>0.05</sub>(MA<sub>0.17</sub>FA<sub>0.83</sub>)<sub>0.95</sub>]<sub>0.95</sub>Pb(Br<sub>0.17</sub>I<sub>0.83</sub>)<sub>3</sub></b> /spiro-OMeTAD/Au	5F-PAI	1.17	24.6	0.79	22.9	10
2021	ITO/PEDOT: PSS/ <b>PEA<sub>0.08</sub>FA<sub>x</sub>SnI<sub>3</sub></b> /C60/BCP/Al	PEAI	0.50	23.1	0.69	7.99	11
Method: Adding organic molecular into precursor							
Year	Device structures	Organic ammonium salt	V <sub>OC</sub> (V)	J <sub>SC</sub> (mA·cm <sup>-2</sup> )	FF	PCE (%)	Ref.
2018	ITO/PEDOT: PSS/ <b>MAPb<sub>0.5</sub>Sn<sub>0.5</sub>I<sub>x</sub>Cl<sub>3-x</sub></b> /PCBM/Phen-NaDPO/Ag	NAP	0.71	27.1	0.70	13.4	12
2021	ITO/PTAA/ <b>FA<sub>0.7</sub>MA<sub>0.25</sub>Cs<sub>0.05</sub>Pb(I<sub>0.93</sub>Br<sub>0.07</sub>)<sub>3</sub></b> /PCBM/BCP/Ag	GBA	1.14	23.5	0.80	21.5	13
Method: spin-coating organic ammonium salt solution onto the surface of the 3D perovskite film							
Year	Device structures	Organic ammonium salt	V <sub>OC</sub> (V)	J <sub>SC</sub> (mA·cm <sup>-2</sup> )	FF	PCE (%)	Ref.
2016	ITO/PEDOT: PSS/ <b>MAPbI<sub>x</sub>Cl<sub>3-x</sub></b> /PCBM/Ag	CAI	0.92	19.3	0.77	13.8	14
2018	FTO/c-TiO <sub>2</sub> /m-TiO <sub>2</sub> / <b>(FAPbI<sub>3</sub>)<sub>0.88</sub>(CsPbBr<sub>3</sub>)<sub>0.12</sub></b> /CuSCN/Au	5-AVA	1.07	21.9	0.72	16.8	15
2018	FTO/SnO <sub>2</sub> / <b>Cs<sub>0.05</sub>(FA<sub>x</sub>MA<sub>1-x</sub>)<sub>0.95</sub>PbI<sub>y</sub>Br<sub>3-y</sub></b> /spiro-OMeTAD/Au	PEAI&PEABr	1.14	23.6	0.74	20.1	16
2018	FTO/TiO <sub>2</sub> / <b>Cs<sub>0.05</sub>(FA<sub>0.83</sub>MA<sub>0.17</sub>)<sub>0.95</sub>Pb(I<sub>0.83</sub>Br<sub>0.17</sub>)</b>	PEAI	1.11	22.9	0.73	18.5	17

J <sub>sc</sub> /spiro-OMeTAD/Au							
	FTO/c-TiO <sub>2</sub> /m-TiO <sub>2</sub> /						
2018	<b>Cs<sub>0.05</sub>(MA<sub>0.17</sub>FA<sub>0.83</sub>)<sub>0.95</sub>Pb(I<sub>0.83</sub>Br<sub>0.17</sub>)<sub>3</sub></b> /spiro-OMeTAD/Au	BAI	1.06	19.4	0.77	15.7	18
2018	FTO/c-TiO <sub>2</sub> /m-TiO <sub>2</sub> / <b>MAPbI<sub>3</sub></b> /spiro-OMeTAD/Au	AVAI	1.06	22.3	0.76	18.0	19
2019	FTO/c-TiO <sub>2</sub> /m-TiO <sub>2</sub> / <b>FAPbI<sub>3</sub></b> /spiro-OMeTAD/Au	FEAI	1.10	25.8	0.78	22.1	20
2019	ITO/TiO <sub>2</sub> / <b>(MA<sub>0.95</sub>Cs<sub>0.05</sub>PbBr<sub>3</sub>)<sub>0.15</sub>(FA<sub>0.95</sub>Cs<sub>0.05</sub>PbI<sub>3</sub>)<sub>0.85</sub></b> /spiro-OMeTAD/Au	VBABr&VBAI	1.15	22.5	0.78	20.2	21
2019	ITO/SnO <sub>2</sub> / <b>Cs<sub>0.17</sub>FA<sub>0.83</sub>Pb(I<sub>0.6</sub>Br<sub>0.4</sub>)<sub>3</sub></b> /spiro-OMeTAD/Au	BAI	1.31	19.3	0.78	19.8	22
2019	ITO/TiO <sub>2</sub> / <b>Cs<sub>0.1</sub>(FA<sub>0.83</sub>MA<sub>0.17</sub>)<sub>0.9</sub>Pb(I<sub>0.83</sub>Br<sub>0.17</sub>)<sub>3</sub></b>	FPEAI	1.13	22.8	0.80	20.5	23
2019	FTO/TiO <sub>2</sub> / <b>FAPbI<sub>3</sub></b> /spiro-OMeTAD/Au	PEAI	1.14	24.2	0.77	21.2	24
2019	FTO/c-TiO <sub>2</sub> &PCBM/ <b>CsPbI<sub>2</sub>Br</b> /spiro-OMeTAD/Au	BAI	1.08	16.8	0.80	14.5	25
2020	FTO/SnO <sub>2</sub> / <b>Cs<sub>x</sub>FA<sub>1-x-y</sub>MA<sub>y</sub>PbI<sub>3-z</sub>Br<sub>z</sub></b> /spiro-OMeTAD/Ag	PNAI	1.16	23.8	0.82	22.6	26
2020	FTO/SnO <sub>2</sub> / <b>Cs<sub>(1-x)</sub>Rb<sub>x</sub>PbI<sub>2</sub>Br</b> /spiro-OMeTAD/Au	GABr	1.25	15.9	0.78	15.6	27
2020	ITO/SnO <sub>2</sub> / <b>CsPbI<sub>x</sub>Br<sub>3-x</sub></b> /spiro-OMeTAD/Au	GABr	1.27	18.0	0.79	18.1	28
2020	FTO/c-TiO <sub>2</sub> /m-TiO <sub>2</sub> /p-TiO <sub>2</sub> / <b>(FAPbI<sub>3</sub>)<sub>0.87</sub>(MAPbBr<sub>3</sub>)<sub>0.13</sub>J<sub>0.92</sub>(CsPbI<sub>3</sub>)<sub>0.08</sub></b> /spiro-OMeTAD/Au	3-TMAI	1.13	23.6	0.77	20.6	29
2020	FTO/SnO <sub>2</sub> / <b>Cs<sub>x</sub>FA<sub>1-x-y</sub>MA<sub>y</sub>PbI<sub>3-z</sub>Br<sub>z</sub></b> /spiro-OMeTAD/Au	HDADI	1.10	22.8	0.81	20.3	30
2020	ITO/PEDOT: PSS/ <b>FA<sub>SnI<sub>3</sub></sub></b> /C60/BCP/Ag	TFBAI	0.70	21.1	0.74	11.0	31
2021	ITO/SnO <sub>2</sub> / <b>FA<sub>1-x</sub>MA<sub>x</sub>PbI<sub>3-y-z</sub>Br<sub>y</sub>Cl<sub>z</sub></b> /spiro-OMeTAD/Au	TFBAI	1.11	24.3	0.78	21.1	32
2021	ITO/SnO <sub>2</sub> / <b>FA<sub>1-x</sub>MA<sub>x</sub>PbI<sub>3-y-z</sub>Br<sub>y</sub>Cl<sub>z</sub></b> /spiro-OMeTAD/Au	CH <sub>3</sub> O-PEAI	1.21	24.3	0.79	23.4	33
2021	ITO/SnO <sub>2</sub> / <b>(FAPbI<sub>3</sub>)<sub>0.95</sub>(MAPbBr<sub>3</sub>)<sub>0.05</sub></b> /spiro-OMeTAD/Au	VBABr	1.14	24.2	0.80	21.9	34
2021	ITO/2PACz/ <b>Cs<sub>0.18</sub>FA<sub>0.82</sub>PbI<sub>3</sub></b> /C60/BCP/Ag	PEACl	1.16	23.5	0.83	22.7	35
2021	FTO/TiO <sub>2</sub> / <b>CsPbI<sub>3-x</sub>Br<sub>x</sub></b> /spiro-OMeTAD/Au	MOPEABr	1.23	20.1	0.82	20.3	36
2021	FTO/TiO <sub>2</sub> / <b>Cs<sub>0.05</sub>FA<sub>0.85</sub>MA<sub>0.10</sub>Pb(I<sub>0.90</sub>Br<sub>0.10</sub>)<sub>3</sub></b>	DMAI	1.16	24.2	0.78	21.9	37
2021	FTO/SnO <sub>2</sub> / <b>FAPbI<sub>3</sub></b> /spiro-OMeTAD/Au	CHMAI	1.14	24.8	0.84	23.9	38
2021	FTO/NbO <sub>x</sub> / <b>MAPbI<sub>3</sub></b> /PCBM/Ag	ABHB	1.10	23.4	0.82	21.2	39
2021	ITO/SnO <sub>2</sub> / <b>Cs<sub>0.05</sub>(FA<sub>0.85</sub>MA<sub>0.15</sub>)<sub>0.95</sub>PbI<sub>3</sub></b> /spiro-OMeTAD/MoO <sub>3</sub> /Ag	EDBE	1.13	24.8	0.81	22.6	40
2021	FTO/TiO <sub>2</sub> / <b>FA<sub>0.85</sub>MA<sub>0.1</sub>Cs<sub>0.05</sub>PbI<sub>2.9</sub>Br<sub>0.1</sub></b> /spiro-	PDAI <sub>2</sub>	1.16	25.3	0.84	24.7	41

OMeTAD/Au							
2022	ITO/SnO <sub>2</sub> / <b>FAPbI<sub>3</sub></b> /spiro-OMeTAD/MoO <sub>3</sub> /Ag	CPAH	1.15	25.5	0.78	22.8	42
Method: spin-coating organic molecular solution onto the surface of the 3D perovskite film							
Year	Device structures	Molecular	V <sub>OC</sub> (V)	J <sub>SC</sub> (mA·cm <sup>-2</sup> )	FF	PCE (%)	Ref.
2017	FTO/TiO <sub>2</sub> / <b>Cs<sub>x</sub>FA<sub>1-x</sub>PbBr<sub>y</sub>I<sub>3-y</sub></b> /spiro-OMeTAD/Au	Benzylamine	1.24	19.8	0.74	18.1	43
Method: Dissolving organic ammonium salt in antisolvent for perovskite film formation							
Year	Device structures	Organic ammonium salt	V <sub>OC</sub> (V)	J <sub>SC</sub> (mA·cm <sup>-2</sup> )	FF	PCE (%)	Ref.
2017	FTO/NiO/ <b>MAPbI<sub>3</sub></b> /(PCBM/PN4N)/Ag	PEAI	1.17	21.8	0.78	19.9	44

**Table S2** Intensity of diffraction peaks at the (100), (110) planes and corresponding ratios for the control and different TFPAI-treated concentrations.

	Control	TFPAI-5	TFPAI-7	TFPAI-9	TFPAI-11	TFPAI-13
$I_{(100)}$	1214	1386	1489	1581	1523	1454
$I_{(110)}$	741	722	693	719	739	731
$I_{(100)}/I_{(110)}$	1.64	1.92	2.15	2.20	2.06	1.99

**Table S3** The PV performance of the devices treated by different concentrations.

Samples	$V_{OC}$ (V)	$J_{SC}$ (mA/cm <sup>2</sup> )	FF (%)	PCE (%)
Control	1.09	23.9	75.9	19.9
TFPAI-5	1.12	23.9	78.9	21.2
TFPAI-7	1.14	24.1	80.2	22.0
TFPAI-9	1.16	24.0	80.8	22.5
TFPAI-11	1.15	23.8	81.1	22.2
TFPAI-13	1.14	24.0	78.6	21.4

**Table S4** The average PV performance of the control and 2D/3D devices.

Samples	$V_{oc}$ (V)	$J_{sc}$ (mA/cm <sup>2</sup> )	FF (%)	PCE (%)
Control	$1.09 \pm 0.02$	$23.7 \pm 0.6$	$75.6 \pm 3.4$	$19.6 \pm 1.1$
2D/3D	$1.14 \pm 0.02$	$23.9 \pm 0.5$	$80.6 \pm 1.5$	$22.1 \pm 0.7$

**Table S5** The Pb:I ration of the control and 2D/3D films calculated by the element sensitivity factor method.

	Control	2D/3D
--	---------	-------

Pb:I	1:1.88	1:2.58
------	--------	--------

**Table S6** Fitting results of the TRPL results.

Samples	A <sub>1</sub>	τ <sub>1</sub> (ns)	A <sub>2</sub>	τ <sub>2</sub> (ns)	τ <sub>ave</sub> (ns)
Control	0.43	5.79	0.56	95.43	91.44
2D/3D	0.29	9.59	0.69	381.98	378.09

**Table S7** Fitting results of the EIS results for the control device.

	R <sub>tr</sub> (Ω)	R <sub>rec</sub> (Ω)
0 V	2.78 × 10 <sup>5</sup>	4.41 × 10 <sup>6</sup>
0.2 V	2.68 × 10 <sup>5</sup>	3.98 × 10 <sup>6</sup>
0.4 V	2.55 × 10 <sup>5</sup>	3.47 × 10 <sup>6</sup>
0.6 V	2.37 × 10 <sup>5</sup>	2.10 × 10 <sup>6</sup>

**Table S8** Fitting results of the EIS results for the 2D/3D device.

	R <sub>tr</sub> (Ω)	R <sub>rec</sub> (Ω)
0 V	1.91 × 10 <sup>5</sup>	5.91 × 10 <sup>6</sup>
0.2 V	1.10 × 10 <sup>5</sup>	5.18 × 10 <sup>6</sup>
0.4 V	8.01 × 10 <sup>4</sup>	3.81 × 10 <sup>6</sup>
0.6 V	6.98 × 10 <sup>4</sup>	2.69 × 10 <sup>6</sup>

## References

1. G. Grancini, C. Roldán-Carmona, I. Zimmermann, E. Mosconi, X. Lee, D. Martineau, S. Narbey, F. Oswald, F. De Angelis, M. Graetzel and M. K. Nazeeruddin, *Nature Communications*, 2017, **8**, 15684.
2. Z. Wang, Q. Lin, F. P. Chmiel, N. Sakai, L. M. Herz and H. J. Snaith, *Nature Energy*, 2017, **2**, 17135.
3. M.-H. Li, H.-H. Yeh, Y.-H. Chiang, U. S. Jeng, C.-J. Su, H.-W. Shiu, Y.-J. Hsu, N. Kosugi, T. Ohigashi, Y.-A. Chen, P.-S. Shen, P. Chen and T.-F. Guo, *Advanced Materials*, 2018, **30**, 1801401.
4. H. Zheng, G. Liu, X. Chen, B. Zhang, A. Alsaedi, T. Hayat, X. Pan and S. Dai, *Journal of Materials Chemistry A*, 2018, **6**, 20233-20241.
5. P. Li, Y. Zhang, C. Liang, G. Xing, X. Liu, F. Li, X. Liu, X. Hu, G. Shao and Y. Song, *Advanced Materials*, 2018, **30**, 1805323.
6. K. T. Cho, Y. Zhang, S. Orlandi, M. Cavazzini, I. Zimmermann, A. Lesch, N. Tabet, G. Pozzi, G. Grancini and M. K. Nazeeruddin, *Nano Letters*, 2018, **18**, 5467-5474.
7. Y. Jiang, J. Yuan, Y. Ni, J. Yang, Y. Wang, T. Jiu, M. Yuan and J. Chen, *Joule*, 2018, **2**, 1356-1368.
8. T. Zhou, H. Lai, T. Liu, D. Lu, X. Wan, X. Zhang, Y. Liu and Y. Chen, *Advanced Materials*, 2019, **31**, 1901242.
9. Q. Yao, Q. Xue, Z. Li, K. Zhang, T. Zhang, N. Li, S. Yang, C. J. Brabec, H.-L. Yip and Y. Cao, *Advanced Materials*, 2020, **32**, 2000571.
10. C. Liang, K. M. M. Salim, P. Li, Z. Wang, T. M. Koh, H. Gu, B. Wu, J. Xia, Z. Zhang, K. Wang, T. Liu, Q. Wei, S. Wang, Y. Tang, G. Shao, Y. Song, N. Mathews and G. Xing, *Journal of Materials Chemistry A*, 2020, **8**, 5874-5881.
11. S. Shao, M. Nijenhuis, J. Dong, S. Kahmann, G. H. ten Brink, G. Portale and M. A. Loi, *Journal of Materials Chemistry A*, 2021, **9**, 10095-10103.
12. Z. Chen, M. Liu, Z. Li, T. Shi, Y. Yang, H.-L. Yip and Y. Cao, *iScience*, 2018, **9**, 337-346.
13. Z. Wang, Y. Lu, Z. Xu, J. Hu, Y. Chen, C. Zhang, Y. Wang, F. Guo and Y. Mai, *Advanced Science*, 2021, **8**, 2101856.
14. C. Ma, C. Leng, Y. Ji, X. Wei, K. Sun, L. Tang, J. Yang, W. Luo, C. Li, Y. Deng, S. Feng, J. Shen, S. Lu, C. Du and H. Shi, *Nanoscale*, 2016, **8**, 18309-18314.
15. J. Chen, J.-Y. Seo and N.-G. Park, *Advanced Energy Materials*, 2018, **8**, 1702714.
16. Y. Lv, Y. Shi, X. Song, J. Liu, M. Wang, S. Wang, Y. Feng, S. Jin and C. Hao, *ACS Applied Materials & Interfaces*, 2018, **10**, 31755-31764.
17. P. Chen, Y. Bai, S. Wang, M. Lyu, J.-H. Yun and L. Wang, *Advanced Functional Materials*, 2018, **28**, 1706923.
18. T. M. Koh, V. Shanmugam, X. Guo, S. S. Lim, O. Filonik, E. M. Herzig, P. Müller-Buschbaum, V. Swamy, S. T. Chien, S. G. Mhaisalkar and N. Mathews, *Journal of Materials Chemistry A*, 2018, **6**, 2122-2128.
19. T. Ye, A. Bruno, G. Han, T. M. Koh, J. Li, N. F. Jamaludin, C. Soci, S. G. Mhaisalkar and W. L. Leong, *Advanced Functional Materials*, 2018, **28**, 1801654.
20. Y. Liu, S. Akin, L. Pan, R. Uchida, N. Arora, V. Milić Jovana, A. Hinderhofer, F. Schreiber, R. Uhl Alexander, M. Zakeeruddin Shaik, A. Hagfeldt, M. I. Dar and M. Grätzel, *Science Advances*, 2019, **5**, eaaw2543.
21. A. H. Proppe, M. Wei, B. Chen, R. Quintero-Bermudez, S. O. Kelley and E. H. Sargent, *Journal of the American Chemical Society*, 2019, **141**, 14180-14189.

22. S. Gharibzadeh, B. Abdollahi Nejand, M. Jakoby, T. Abzieher, D. Hauschild, S. Moghadamzadeh, J. A. Schwenzer, P. Brenner, R. Schmager, A. A. Haghimirad, L. Weinhardt, U. Lemmer, B. S. Richards, I. A. Howard and U. W. Paetzold, *Advanced Energy Materials*, 2019, **9**, 1803699.
23. Q. Zhou, L. Liang, J. Hu, B. Cao, L. Yang, T. Wu, X. Li, B. Zhang and P. Gao, *Advanced Energy Materials*, 2019, **9**, 1802595.
24. T. Niu, J. Lu, X. Jia, Z. Xu, M.-C. Tang, D. Barrit, N. Yuan, J. Ding, X. Zhang, Y. Fan, T. Luo, Y. Zhang, D.-M. Smilgies, Z. Liu, A. Amassian, S. Jin, K. Zhao and S. Liu, *Nano Letters*, 2019, **19**, 7181-7190.
25. M. Tai, Y. Zhou, X. Yin, J. Han, Q. Zhang, Y. Zhou and H. Lin, *Journal of Materials Chemistry A*, 2019, **7**, 22675-22682.
26. M. He, J. Liang, Z. Zhang, Y. Qiu, Z. Deng, H. Xu, J. Wang, Y. Yang, Z. Chen and C.-C. Chen, *Journal of Materials Chemistry A*, 2020, **8**, 25831-25841.
27. W. Zhang, J. Xiong, J. Li and W. A. Daoud, *Solar RRL*, 2020, **4**, 2000112.
28. Y. Zheng, X. Yang, R. Su, P. Wu, Q. Gong and R. Zhu, *Advanced Functional Materials*, 2020, **30**, 2000457.
29. A. A. Sutanto, N. Drigo, V. I. E. Queloz, I. Garcia-Benito, A. R. Kirmani, L. J. Richter, P. A. Schouwink, K. T. Cho, S. Paek, M. K. Nazeeruddin and G. Grancini, *Journal of Materials Chemistry A*, 2020, **8**, 2343-2348.
30. Y. Lv, H. Ma, Y. Yin, Q. Dong, W. Zhao, S. Jin and Y. Shi, *Journal of Materials Chemistry A*, 2020, **8**, 10283-10290.
31. T. Wu, D. Cui, X. Liu, X. Meng, Y. Wang, T. Noda, H. Segawa, X. Yang, Y. Zhang and L. Han, *Solar RRL*, 2020, **4**, 2000240.
32. J. Xia, C. Liang, S. Mei, H. Gu, B. He, Z. Zhang, T. Liu, K. Wang, S. Wang, S. Chen, Y. Cai and G. Xing, *Journal of Materials Chemistry A*, 2021, **9**, 2919-2927.
33. J. Zhuang, P. Mao, Y. Luan, N. Chen, X. Cao, G. Niu, F. Jia, F. Wang, S. Cao and J. Wang, *Advanced Functional Materials*, 2021, **31**, 2010385.
34. A. H. Proppe, A. Johnston, S. Teale, A. Mahata, R. Quintero-Bermudez, E. H. Jung, L. Grater, T. Cui, T. Filleter, C.-Y. Kim, S. O. Kelley, F. De Angelis and E. H. Sargent, *Nature Communications*, 2021, **12**, 3472.
35. S. Gharibzadeh, P. Fassl, I. M. Hossain, P. Rohrbeck, M. Frericks, M. Schmidt, T. Duong, M. R. Khan, T. Abzieher, B. A. Nejand, F. Schackmar, O. Almora, T. Feeney, R. Singh, D. Fuchs, U. Lemmer, J. P. Hofmann, S. A. L. Weber and U. W. Paetzold, *Energy & Environmental Science*, 2021, DOI: 10.1039/D1EE01508G.
36. S. Zhang, L. Zhang, Q. Tian, X. Gu, Y. Du, K. Zhao and S. Liu, *Advanced Energy Materials*, 2021, **n/a**, 2103007.
37. J. Sun, X. Zhang, X. Ling, Y. Yang, Y. Wang, J. Guo, S. Liu, J. Yuan and W. Ma, *Journal of Materials Chemistry A*, 2021, **9**, 23019-23027.
38. S. Jeong, S. Seo, H. Yang, H. Park, S. Shin, H. Ahn, D. Lee, J. H. Park, N.-G. Park and H. Shin, *Advanced Energy Materials*, 2021, **11**, 2102236.
39. R. Garai, R. K. Gupta, M. Hossain and P. K. Iyer, *Journal of Materials Chemistry A*, 2021, **9**, 26069-26076.
40. T. Niu, Y.-M. Xie, Q. Xue, S. Xun, Q. Yao, F. Zhen, W. Yan, H. Li, J.-L. Brédas, H.-L. Yip and Y. Cao, *Advanced Energy Materials*, 2021, **n/a**, 2102973.
41. F. Zhang, Y. Park So, C. Yao, H. Lu, P. Dunfield Sean, C. Xiao, S. Uličná, X. Zhao, L. Du Hill, X. Chen, X. Wang, E. Mundt Laura, H. Stone Kevin, T. Schelhas Laura, G. Teeter, S. Parkin, L. Ratcliff Erin, Y.-

- L. Loo, J. Berry Joseph, C. Beard Matthew, Y. Yan, W. Larson Bryon and K. Zhu, *Science*, 2022, **375**, 71-76.
42. J. Wang, L. Liu, S. Chen, G. Ran, W. Zhang, M. Zhao, C. Zhao, F. Lu, T. Jiu and Y. Li, *Nano Today*, 2022, **42**, 101357.
43. Y. Zhou, F. Wang, Y. Cao, J.-P. Wang, H.-H. Fang, M. A. Loi, N. Zhao and C.-P. Wong, *Advanced Energy Materials*, 2017, **7**, 1701048.
44. Y. Bai, S. Xiao, C. Hu, T. Zhang, X. Meng, H. Lin, Y. Yang and S. Yang, *Advanced Energy Materials*, 2017, **7**, 1701038.